

Ultrarelativistic electromagnetic counterpart to binary neutron star mergers

Koutarou Kyutoku¹, Kunihiro Ioka^{2,3} and Masaru Shibata⁴

¹*Department of Physics, University of Wisconsin-Milwaukee, PO Box 413, Milwaukee, WI 53201, USA*

²*Theory Center, Institute of Particles and Nuclear Studies, KEK, Tsukuba 305-0801, Japan*

³*Department of Particle and Nuclear Physics, the Graduate University for Advanced Studies (Sokendai), Tsukuba 305-0801, Japan*

⁴*Yukawa Institute for Theoretical Physics, Kyoto University, Kyoto 606-8502, Japan*

1 November 2018

ABSTRACT

We propose a possibility of ultrarelativistic electromagnetic counterparts to gravitational waves from binary neutron star mergers at nearly all the viewing angles. Our proposed mechanism relies on the merger-shock propagation accelerating a smaller mass in the outer parts of the neutron star crust to a larger Lorentz factor Γ with smaller energy $\sim 10^{47}\Gamma^{-1}$ erg. This mechanism is difficult to resolve by current 3D numerical simulations. The outflows emit synchrotron flares for seconds to days by shocking the ambient medium. Ultrarelativistic flares shine at an early time and in high-energy bands, potentially detectable by current X-ray to radio instruments, such as *Swift* XRT and Pan-STARRS, and even in low ambient density $\sim 10^{-2}\text{ cm}^{-3}$ by EVLA. The flares probe the merger position and time, and the merger types as black hole–neutron star outflows would be non-/mildly relativistic.

Key words: gravitational waves — radiation mechanisms: non-thermal — shock waves — binaries: close — stars: neutron

1 INTRODUCTION

Binary neutron star (BNS) mergers are main sources of gravitational waves (GWs) for ground-based laser-interferometric detectors, such as advanced LIGO, advanced Virgo and KAGRA in the coming five years (Abadie et al. 2010a; Kuroda et al. 2010; Accadia et al. 2011). GW detection will open a new window for astronomy, and we will be able to test the theory of gravitation and to probe the supranuclear-density matter in neutron stars (NSs). Statistical studies suggest that a few tens of merger events are observed in a year within a few hundred Mpc distance (Abadie et al. 2010b).

A simultaneous detection of electromagnetic (EM) signals is indispensable for declaring a confident discovery of GWs (Metzger & Berger 2012; Piran et al. 2013). Since ‘hearing’ a sound of GWs entails a bad localization about degree² at best, ‘seeing’ EM counterparts will not only increase GW sensitivity but also expand *multi messenger astronomy* by extracting information such as the host galaxy and its redshift.

Short γ -ray bursts (SGRBs) are plausible counterparts to BNS mergers (Nakar 2007). GWs will verify the merger hypothesis for SGRBs. However, some observations suggest that SGRBs are beamed into a small angle (Fong et al. 2012). Most SGRBs are off-axis and undetectable to us, albeit GW observation is biased towards the binary’s rota-

tional axis (i.e., probably the jet axis). The ‘orphan’ afterglow, which is produced by the off-axis jet decelerated to a mildly relativistic velocity at a later time, is also dim.

Two promising models have been proposed for nearly isotropic EM counterparts. One is the macronova or kilonova which shines on \sim days after the merger in UV–optical bands via radioactive decay of r -process elements (Li & Paczyński 1998; Kurkarni 2005; Metzger et al. 2010). The other is radio synchrotron emission from the collisions between the ejecta and the ambient medium, like γ -ray burst (GRB) afterglows, after \sim years from the merger (Nakar & Piran 2011). Both of them are based on non-/mildly relativistic outflows with ~ 0.2 – $0.3c$ (roughly an escape velocity of the NS) from a compact binary merger. The outflows can be produced by neutrino-driven wind (Dessart et al. 2009), magnetically driven wind (Shibata et al. 2011; Kiuchi et al. 2012), tidal ejection (Roberts et al. 2011) and shock-wave ejection (Goriely et al. 2011) (see also below). Recent fully general relativistic simulations show that the ejecta mass is $\gtrsim 10^{-3}M_{\odot}$ for a wide range of parameters even without neutrino or magnetic effects (Hotokezaka et al. 2013).

In this Letter, we suggest a possibility of nearly omnidirectional ultrarelativistic counterparts to BNS mergers for the first time to our knowledge except for the GRB. We consider shock waves produced right after the BNS collision (Sekiguchi et al. 2011; Paschalidis et al. 2012). Shock

waves are launched from the heated NS core to the NS crust non-relativistically at first, and accelerate to a relativistic velocity down a steep density gradient in the NS crust. After the shock breakout from the surface, the shocked material expands into a nearly vacuum region, converting the shock-heated internal energy into kinetic energy. The resulting Lorentz factor Γ of the ejecta is larger for outer and less massive parts. Such a transrelativistic acceleration has been discussed in the context of supernovae (Sakurai 1960; Johnson & Mckee 1971; Matzner & Mckee 1999; Tan et al. 2001; Pan & Sari 2006).

We estimate the relativistic ejecta mass to be $\sim 10^{-7}\Gamma^{-2}M_{\odot}$ for $\Gamma \gg 1$, and calculate the synchrotron radiation from relativistic blast waves decelerated by the ambient medium and energized progressively by the inner catching-up ejecta. The ultrarelativistic nature makes the flare bright at an early time (seconds–days) and in high-energy bands (X-ray–radio bands) in contrast to the non-/mildly relativistic cases. We find flares are detectable by current X-ray, optical and radio instruments, such as *Swift* XRT, Pan-STARRS and EVLA for our fiducial case.

The counterpart signals the merger time more precisely than non-/mildly relativistic ones. The counterpart could also enable us to distinguish the merger types, because black hole–NS mergers are not likely to be accompanied by strong shocks for ultrarelativistic outflows.

Current 3D numerical simulations of BNS mergers have not sufficiently resolved the NS crust. Although the results for non-/mildly relativistic ejecta are solid and the existence of shock waves is implied by the heatup of the colliding region (Sekiguchi et al. 2011; Paschalidis et al. 2012); currently, it is not feasible to follow a tiny mass to a ultrarelativistic velocity because of numerical viscosity, artificial atmosphere and limited computational resources, even for Newtonian gravity. Therefore, it is worthwhile to highlight the impacts of ultrarelativistic outflows for motivating the future well-resolved calculations.

2 ACCELERATION

We first consider the mass ejection right after the NS collision. The NSs collide with each other due to the gravitational radiation reaction. The colliding part is shock heated up to a temperature of ~ 50 MeV. Because of an oblique collision, the shocked region has a pancake-like shape with the thickness $R_{\text{sh}} \sim O(1)$ km (Sekiguchi et al. 2011; Paschalidis et al. 2012), as shown in Fig. 1.

The hot material in the colliding region expands towards a cold, low-pressure region, i.e., from the heated NS core to the NS crust. The striking difference of the pressure between them drives shock waves propagating the NS crust towards an NS surface. The initial shock velocity v_{ini} should be comparable to the sound velocity of the core material $\sim 0.25c$ (Oertel et al. 2012), where c is the speed of light. At this stage, the shocked material cannot escape from the merged remnant, because the expanding velocity is less than the escape velocity,

$$v_{\text{esc}} \approx 0.74c \left(\frac{M_*}{2.8M_{\odot}} \right)^{1/2} \left(\frac{R_*}{15 \text{ km}} \right)^{-1/2}, \quad (1)$$

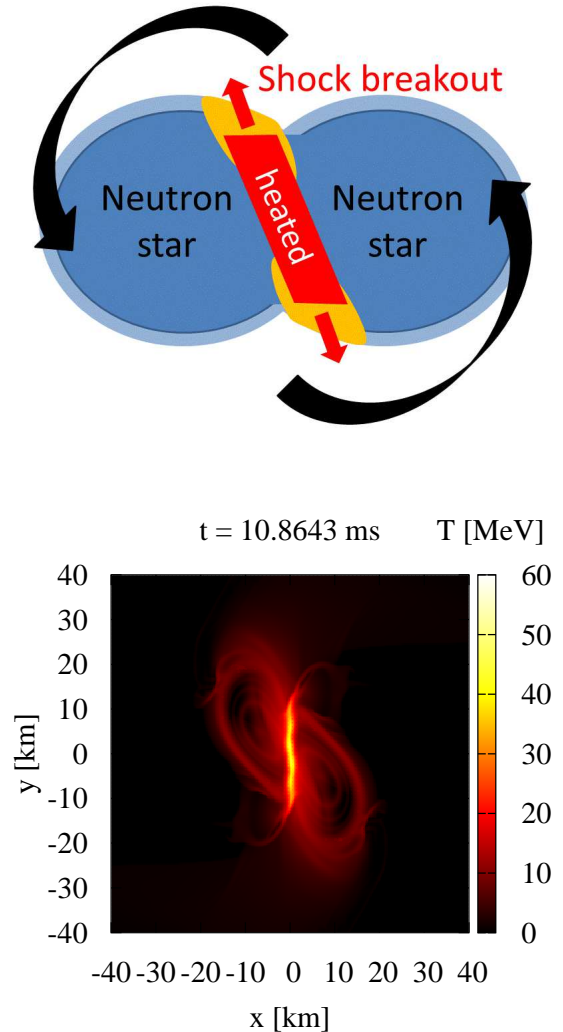


Figure 1. Top: a schematic picture of the shock generation, propagation and mass ejection right after the BNS merger. Two blue ellipses are the BNS with a low temperature and the low-density crust is depicted with light blue. A red region at the contact surface is the shock-heated region. The black arrows denote the BNS motion just before the merger. Shock waves are generated from the contact of the BNS. The shocks become strong in the NS crust and eject a part of the NS crust ultrarelativistically. Bottom: a snapshot of merging BNS with $1.5 M_{\odot}$ taken from a simulation in Sekiguchi et al. (2011). The temperature on the equatorial plane is shown, and the contact surface is heated up to ~ 50 MeV.

where M_* and R_* are the mass and radius of the merged remnant, respectively.

The shock is accelerated descending a steep density gradient in the NS crust with the thickness $R_c \approx 1$ km. The density profile of the crust is approximately given by $\rho \propto x^n$, where ρ is the rest-mass density, x is the depth from the surface and n is the polytropic index of the crust equation of state (EOS). We adopt $n = 3$ as a fiducial value, because this is for the relativistic degenerate electron gas and is consistent with more detailed nuclear-theory-based EOSs (Chamel & Haensel 2008).

The shock velocity increases as $\propto \rho^{-\alpha}$ with $\alpha \approx 0.187$

for $n = 3$ in the non-relativistic regime (Sakurai 1960). Once the shock is accelerated beyond $\approx 0.5v_{\text{esc}}$, the shocked material can escape from the BNS by converting thermal energy into kinetic energy to obtain $\approx v_{\text{esc}}$ later (Sakurai 1960; Matzner & Mckee 1999). Specifically, the shock velocity increases by a factor of $0.5v_{\text{esc}}/v_{\text{ini}} \sim 1.5$ when the density drops by $1.5^{-1/\alpha} \approx 0.1$. The crust material outside this density can escape as ejecta. For $\rho \propto x^n$, the ejecta mass is estimated to be

$$M_{\text{sh}} \approx M_c \left(\frac{R_{\text{sh}}}{R_*} \right) \left(\frac{0.5v_{\text{esc}}}{v_{\text{ini}}} \right)^{-(n+1)/n\alpha} \\ \approx 4.4 \times 10^{-5} M_{\odot} \left(\frac{v_{\text{ini}}}{0.25c} \right)^{7.1} \left(\frac{v_{\text{esc}}}{0.74c} \right)^{-7.1}, \quad (2)$$

where $R_{\text{sh}}/R_* \approx 1 \text{ km}/15 \text{ km}$ is a geometrical fraction of the crust mass $M_c \approx 0.01M_{\odot}$ that is swept by the shock (Fig. 1).

The ejecta is approximately spherical. The reason for this is that the shock is initially non-relativistic, and therefore expands into an angle given by the inverse of the Lorentz factor, $O(1)$. No confinement mechanism works. Since the ejecta geometry is not jet-like but annular, where the annulus is ejected in the yz plane for the bottom panel of Fig. 1, the solid angle is $2\pi \times O(1)$.

The outer and less massive ejecta accelerates to a ultra-relativistic velocity. Specifically, the shock attains a Lorentz factor $\Gamma_s \sim 10$ when the density drops by a factor of $\sim \Gamma_s^{2+4/n\sqrt{3}} \sim 10^4$ within a thin layer of $\sim R_c/\Gamma_s^{(2+4/\sqrt{3})/n} \sim R_c/30$ (Johnson & Mckee 1971; Pan & Sari 2006). Then, after the breakout from the surface, the shocked material accelerates to a Lorentz factor $\Gamma \sim \Gamma_s^{1+\sqrt{3}} \gtrsim 500$ by converting the shock-heated internal energy into the kinetic energy with the aid of the pressure of the inner ejecta. To resolve the thin layer of $\lesssim R_c/30$ in mesh-based simulations, a grid size of $\lesssim 10 \text{ m}$ is required. Such a high-resolution simulation is not feasible at present and in the near-future.

To make a detailed estimate, we apply a transrelativistic acceleration model of a supernova exploding the stellar envelope (Tan et al. 2001). The kinetic energy of ejecta with a velocity above $\beta\Gamma$, where βc is the ejecta velocity, is given by equation 56 of Tan et al. (2001) as¹

$$E(>\beta\Gamma) = \left(\frac{v_{\text{esc}}}{0.58c} \right)^{(n+1)/n\alpha} F(\beta\Gamma) M_{\text{sh}} c^2. \quad (3)$$

An exact form of the distribution $F(\beta\Gamma)$ is given by equation 38 of Tan et al. (2001). Neither gravity nor rotation is expected to affect the shock and post-shock acceleration, since the shock crosses the crust in $O(10)\mu\text{s}$, which is much shorter than the dynamical time-scale and rotational period at the mass-shedding limit, $O(1) \text{ ms}$. The heatup of the stellar interior will take $O(100)\mu\text{s}$, which might require detailed modelling.

Fig. 2 shows the kinetic energy distribution of the ejecta $E(>\beta\Gamma)$. The energy of ultrarelativistic ejecta $E(>\beta\Gamma \approx \Gamma = 10)$ is $\gtrsim 10^{46}$ erg for our fiducial case. For $\beta\Gamma \gg 1$, Eq. (3) yields

$$E(>\Gamma) \approx 2.6 \times 10^{47} \text{ erg} (\Gamma^{-0.94} + \Gamma^{-0.20})^{5.5} \left(\frac{M_{\text{sh}}}{4.4 \times 10^{-5} M_{\odot}} \right), \quad (4)$$

where we assume $M_* = 2.8M_{\odot}$, $R_* = 15 \text{ km}$ and $n = 3$. The

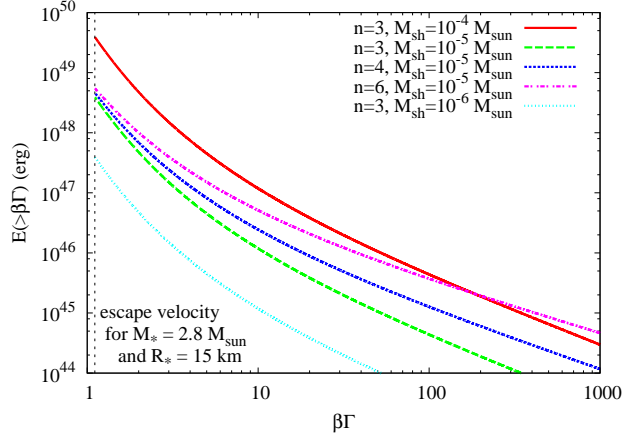


Figure 2. The kinetic energy distribution of ejecta with a velocity larger than $\beta\Gamma$ for various polytropic indices n and the ejected mass by the shock breakout M_{sh} . We assume $M_* = 2.8M_{\odot}$ and $R_* = 15 \text{ km}$.

high- Γ component carries small but still appreciable energy for the emission as $E(>\Gamma) \propto \Gamma^{-0.58-1.58/n} \sim \Gamma^{-1.1}$, while the mass is tiny as $\sim 10^{-7}\Gamma^{-2.1} M_{\odot}$. The energy distribution becomes harder for a larger value of n , providing a possible way to infer the EOS of the NS crust in principle.

The energy distribution is sensitive to the value of M_{sh} , and therefore v_{ini} and the polytropic index, n . The density profile could be affected by the neutrino/magnetic wind, and the shock acceleration will not work efficiently when the density has a stellar-wind-like profile and does not go to zero rapidly. The breakdown of plane-parallel approximation in Tan et al. (2001) could modify the Γ distribution (but see their section 2.5 for aspherical explosions). Some part of the ultrarelativistic ejecta may be decelerated before emission by surrounding material such as a tidally elongated NS, especially for an unequal-mass binary. The neutrino losses may decrease the acceleration pressure (but other radiation components persist). The accurate estimation of M_{sh} and the Γ distribution taking these caveats is left for future study.

The ejecta may be also accelerated when density waves propagate across the entire core to the opposite surface. The amount of shock-breakout ejection would be larger by an order of magnitude due to a larger geometrical fraction. Whether density waves propagate across the core depends on the NS structure, and thus on the EOS of the NS core.

3 RADIATION

Next, we calculate the spectra and light curves of EM signals applying the synchrotron shock model of the GRB afterglow (Sari et al. 1998; Ioka & Mészáros 2005). The outflow generates a forward shock sweeping the ambient medium with a constant number density n_{H} . A fraction $\epsilon_B \sim 0.01$ of the internal energy released by the shock amplifies the magnetic field B , while a fraction $\epsilon_e \sim 0.1$ accelerates electrons with a Lorentz factor distribution $dN_e/d\gamma_e \propto \gamma_e^{-p}$, where N_e and γ_e are the number and Lorentz factor of electrons, respectively, for $\gamma_e \geq \gamma_m$ (a minimum value) and $p \approx 2.2$.

Hereafter, we assume that the ejecta outspreads completely spherically, and give the lower limit of luminosity. If

¹ We adopt $f_{\text{sph}} = 0.85$ and $C_{\text{nr}} = 2.03$ in Tan et al. (2001).

the ejecta is concentrated within an angle θ from the annular heated region, an observable angle decreases by $\approx \theta/\pi$ but the isotropic energy increases by $\approx \pi/\theta$ for a BNS merger, and finally detection rates will increase by $\approx \sqrt{\pi/\theta}$. Our fiducial model can be detected up to $\gtrsim 200$ Mpc for optimal observational bands and the value of n_H , as shown later.

The outflow carries larger energy in inner, lower Γ part in Eqs. (3) and (4). The slow flow rear-ends and refreshes the external shock which is decelerated by the ambient density (Rees & Mészáros 1998; Sari & Mészáros 2000). We illustrate formulae for a power-law distribution of the kinetic energy,

$$E(>\Gamma) = \tilde{E}\Gamma^{1-s}, \quad (5)$$

where $\tilde{E} = 2.6 \times 10^{47}$ erg and $s = 2.1$ for our fiducial case with $\Gamma \gg 1$, and \tilde{E} and s rise as Γ drops in equation (4). We also adopt an ultrarelativistic approximation, $\Gamma \gg 1$. Note that γ_m and B are both proportional to Γ in this approximation. Once the fastest flow begins to decelerate, the catching-up condition for a slower flow is given by $\tilde{E}\Gamma^{1-s} = 16\pi\Gamma^2 R^3 n_H m_p c^2 / 17$ (Blandford & McKee 1976; Sari & Mészáros 2000), where m_p is the proton mass and R is the shock radius. Since the shock radius is connected with the observer time t by $R \approx 4\Gamma^2 ct$ (Sari et al. 1998), we obtain the hydrodynamic evolutions

$$\Gamma(t) = (ct/\ell_S)^{-3/(s+7)}, \quad R(t) = 4\Gamma(t)^2 ct, \quad (6)$$

where $\ell_S \equiv (17\tilde{E}/1024\pi n_H m_p c^2)^{1/3}$ is the Sedov length. Note that $\Gamma \propto t^{-0.33}$ and $R \propto t^{0.34}$ for our fiducial value $s = 2.1$, compared to $\Gamma \propto t^{-3/8}$ and $R \propto t^{1/4}$ for a single-velocity shell.

Given the hydrodynamics above, we can calculate the evolution of radiation (Sari et al. 1998; Ioka & Mészáros 2005). The synchrotron flux has a broken power-law spectrum, $F_\nu \propto \nu^{1/3}$ for $\nu < \nu_m$ and $F_\nu \propto \nu^{-(p-1)/2} \approx \nu^{-0.6}$ for $\nu > \nu_m$, where $\nu_m \propto \gamma_m^2 \Gamma B \propto \Gamma^4 \propto t^{-12/(s+7)}$ is the characteristic synchrotron frequency. The cooling frequency is high ($> \text{MeV}$) for typical parameters. The self-absorption frequency is only relevant for the radio band with $n_H \gtrsim 1 \text{ cm}^{-3}$. For a given frequency ν , the flux reaches the maximum value $F_{\nu,m} \propto N_e \gamma_m^2 \Gamma^2 B^2 / \nu_m$ as ν_m crosses ν , with $N_e \propto R^3$. The peak time and flux are given by

$$t_{\text{peak}} = 6.2 \text{ ms } \epsilon_{e,-1}^{1.52} \epsilon_{B,-2}^{0.38} \tilde{E}_{47}^{1/3} n_{H,0}^{0.05} \nu_{18}^{-0.76}, \quad (7)$$

$$F_{\text{peak}} = 0.21 \mu\text{Jy } \epsilon_{e,-1}^{0.55} \epsilon_{B,-2}^{0.64} \tilde{E}_{47}^{0.64} n_{H,0}^{0.64} D_2^{-2} \nu_{18}^{-0.28}, \quad (8)$$

where $Q_x \equiv Q/10^x$ in units of erg for \tilde{E} , Mpc for D , cm^{-3} for n_H and Hz for ν . The flux grows as $F_\nu \propto t^{(3s+1)/(s+7)} \approx t^{0.80}$ and decays as $F_\nu \propto t^{3(s+1-2p)/(s+7)} \approx t^{-0.43}$ across the peak. These light-curve behaviours could constrain the Γ distribution, i.e., s , and hence the crust EOS, $n \approx 1.58/(s-1.58)$, in principle. The degeneracy between n and p is solved by the high-energy spectral index, $F_\nu \propto \nu^{-(p-1)/2}$.

Fig. 3 shows the light curves in X-ray, optical and radio bands using the (non-power-law) velocity distribution in Eqs. (3) and (4) with various ambient densities n_H . In contrast to the non-/mildly relativistic cases, i.e., optical macronovae/kilonovae and radio flares, the ultrarelativistic signals appear in the early phase down to seconds and in the high frequency up to X-ray. The X-ray and optical peaks correspond to $\Gamma \approx 400$ and 70, respectively.

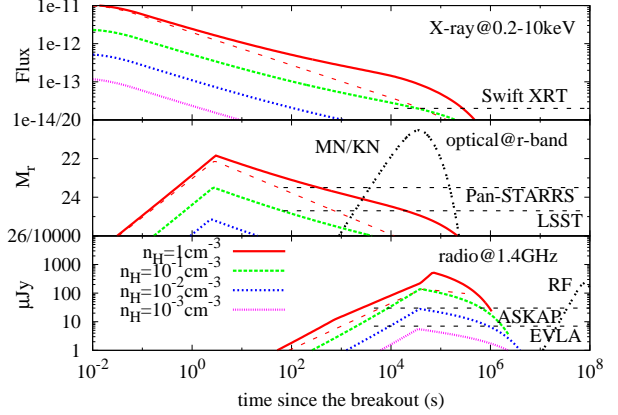


Figure 3. Light curves of the ultrarelativistic EM counterpart with $\tilde{E} = 2.6 \times 10^{47}$ erg at 100 Mpc distance in the X-ray (0.2–10 keV integrated flux in $\text{erg cm}^{-2} \text{s}^{-1}$), optical (in 629 nm, r -band magnitude) and radio (1.4 GHz in μJy) bands for various values of n_H down to $\Gamma \approx 1$. Long dashed red curves are the analytic approximations with the power-law distribution in Eq. (5) with $n_H = 1 \text{ cm}^{-3}$. Short dashed black lines are sensitivity curves of *Swift* XRT, Pan-STARRS, LSST, ASKAP and EVLA. Double dotted black curves in the middle (labelled as MN/KN) and bottom (RF) panels show the non-relativistic EM counterparts of the macronova/kilonova (Li & Paczyński 1998) and the radio flare (Piran et al. 2013), respectively, with the ejecta mass $10^{-3} M_\odot$, ejecta velocity $0.2c$ and $n_H = 1 \text{ cm}^{-3}$. For the macronova/kilonova, the heating efficiency and opacity are taken to be 3×10^{-6} and $0.1 \text{ cm}^2 \text{ g}^{-1}$, respectively (Metzger et al. 2010).

4 DISCUSSION

The ultrarelativistic counterpart proposed here is bright from the early epoch soon after the BNS merger, and decays rapidly. While this feature is advantageous to confirm a tight association with GWs, the observation will require efficient strategies. One such strategy is full-time EM monitoring of nearby (up to ~ 100 Mpc) galaxies, where the EM signals trigger the GW analyses like the SGRB case. The method is expensive, but enables us to discover many other transients including supernovae as a by-product.

The other strategy is prompt follow-up by EM instruments in response to rapid alerts from GW detector networks. The localization requires at least three and hopefully more than four GW detectors. Because a localization error will be $\sim 1 \text{ degree}^2$ at best for a BNS merger (Fairhurst 2011), covering this large area is crucial for the EM follow-up. This will be challenging but not impossible. *Swift* XRT has 0.15 degree^2 field of view (FOV). Tiling the FOV will allow us to detect the decaying phase of the X-ray signal, although the required number of tiles is $\gtrsim 10$. The latency from GW detection to follow-up observation, which could be ~ 12 h (Evans et al. 2012), should be reduced as possible for efficient tiling. Detecting the X-ray peak may be possible if EM precursors are observed in advance (e.g., Ioka & Taniguchi 2000). The optical flare can be observed around its peak by all-sky surveys, such as Pan-STARRS with 7 degree^2 FOV and LSST with 9.6 degree^2 FOV, if $n_H \gtrsim 10^{-1} \text{ cm}^{-3}$. The radio flare can be also detected around the peak by EVLA even in low ambient den-

sity $n_{\text{H}} \approx 10^{-2} \text{ cm}^{-3}$. The low ambient density is suggested by the radio observations of SGRBs (Berger 2010). Since EVLA has relatively small FOV of 0.25 degree^2 , large FOV instruments such as ASKAP with 30 degree^2 FOV may be more realistic choices. Follow-up observation in optical and radio bands has also to be performed as rapid as possible after GW detection to cover the localization error efficiently during bright emission. Detecting the short-lived emission proposed in this Letter will be more challenging for typical localization errors, $10\text{--}100 \text{ degree}^2$ dependent on the detector network configuration, than for optimistic localization errors, $\sim 1 \text{ degree}^2$.

We expect that these detectors will always find the emission by fully covering the GW localization error region if it is $\sim 1 \text{ degree}^2$, which might be possible for the merger at 100 Mpc. The detection probability may be estimated by the fraction of the error region that follow-up observations can cover before the emission fades away. Assuming $n_{\text{H}} = 1 \text{ cm}^{-3}$, XRT, LSST and EVLA will detect the emission up to $\sim 10^5, 10^4$ and 10^6 s after the merger at 100 Mpc, respectively. The number of available pointings and the total FOV is estimated by comparing these values to required integration time of each detector, and the probability is found. By contrast, if the localization error is $\gtrsim 10 \text{ degree}^2$ or the emission is dimmer due to a larger distance or lower ambient density, XRT might find the emission only $\lesssim 10\%$ of the events. LSST and EVLA will be able to detect the emission even in such cases. We would not like to be conclusive at this point, however, due to enormous uncertainties associated with the ambient density, GW localization errors including shapes of them, and the delay from GW detection to follow-up observations.

We also speculate that GeV–TeV γ -rays could be generated via inverse Compton scatterings or hadronic processes, such as $p\text{--}\gamma$ collisions. If energy E_{γ} is converted to γ -rays with typical energy e_{γ} , an expected number of photons N_{γ} for a detector with area A on the earth will be

$$N_{\gamma} \approx 50 \left(\frac{E_{\gamma}}{10^{45} \text{ erg}} \right) \left(\frac{100 \text{ GeV}}{e_{\gamma}} \right) \left(\frac{A}{1 \text{ km}^2} \right) D_2^{-2}. \quad (9)$$

This suggests that km^2 future instruments such as CTA could also detect EM signals in γ -rays. The TeV γ -rays are not attenuated by the infrared background at ~ 100 Mpc.

Ultrarelativistic outflows could also be produced by other mechanisms such as the Poynting wind from the NS surface with a small baryon load like in the magnetar models for GRBs (Metzger et al. 2011). In this case, the EM signals could arise from the magnetic reconnection without the radioactivity or the ambient medium.

Before closing this section, we again summarize the caveats of our model and necessary studies in the future. Our proposed ejection mechanism is based on analytically idealized shock and post-shock acceleration. Local plane-parallel geometry is assumed for a restricted region depicted in Fig. 1 to apply a model in Tan et al. (2001), and the ejecta is assumed to be isotropic relying only on the fact that the shock is initially non-relativistic. The validity of these assumptions has to be confirmed by numerical simulations with grid resolutions $\lesssim 10$ m in the future. We neglected the gravity and rotation based on the time-scale comparison, and this assumption requires more quantitative validation by the simulations. Possible modification of the crustal density pro-

file and screening of ultrarelativistic ejecta by other ejection mechanisms has also to be investigated.

ACKNOWLEDGEMENTS

We are grateful to Akira Mizuta and Hajime Takami for valuable discussion, and to Kenta Kiuchi for providing the bottom panel of Fig. 1. We also thank our referee for helpful comments. This work was supported by the Grant-in-Aid for Scientific Research No. 21684014, 22244030, 24000004, 24103006, and 24244028 of Japanese MEXT and JSPS Postdoctoral Fellowship for Research Abroad.

REFERENCES

- Abadie J. et al., 2010a, Nucl. Instrum. Methods Phys. Res., Sect. A, 624, 223
 Abadie J. et al., 2010b, Class. Quantum Grav., 27, 173001
 Accadia T. et al., 2011, Class. Quantum Grav., 28, 025005
 Berger E., 2010, ApJ, 722, 1946
 Blandford R. D., Mckee C. F., 1976, Phys. Fluids., 19, 113
 Chamel N., Haensel P., 2008, Living Rev. Relativ., 11, 10
 Dessart L., Ott C. D., Burrows A., Rosswog S., Livne E., 2009, ApJ, 690, 1681
 Evans P. A. et al., 2012, ApJS, 203, 28
 Fairhurst S., 2011, Class. Quantum Grav., 28, 105021
 Fong W. et al., 2012, ApJ, 756, 189
 Goriely S., Bauswein A., Janka H.-T., 2011, ApJ, 738, L32
 Hotokezaka K., Kiuchi K., Kyutoku K., Okawa H., Sekiguchi Y.-i., Shibata M., Taniguchi K., 2013, Phys. Rev. D, 87, 024001
 Ioka K., Mészáros P., 2005, ApJ, 619, 684
 Ioka K., Taniguchi K., 2000, ApJ, 537, 327
 Johnson M. H., Mckee C. F., 1971, Phys. Rev. D, 3, 858
 Kiuchi K., Kyutoku K., Shibata M., 2012, Phys. Rev. D, 86, 064008
 Kurkarni S. R., 2005, preprint (astro-ph/0510256)
 Kuroda K. et al., 2010, Class. Quantum Grav., 27, 084004
 Li L.-X., Paczyński B., 1998, ApJ, 507, L59
 Matzner C. D., Mckee C. F., 1999, ApJ, 510, 379
 Metzger B. D., Berger E., 2012, ApJ, 746, 48
 Metzger B. D., Giannios D., Thompson T. A., Bucciantini N., Quataert E., 2011, MNRAS, 413, 2031
 Metzger B. D. et al., 2010, MNRAS, 406, 2650
 Nakar E., 2007, Phys. Rep., 442, 166
 Nakar E., Piran T., 2011, Nat, 478, 82
 Oertel M., Fantina A. F., Novak J., 2012, Phys. Rev. C, 85, 055806
 Pan M., Sari R., 2006, ApJ, 643, 416
 Paschalidis V., Etienne Z. B., Shapiro S. L., 2012, Phys. Rev. D, 86, 064032
 Piran T., Nakar E., Rosswog S., 2013, MNRAS, 430, 2121
 Rees M. J., Mészáros P., 1998, ApJ, 496, L1
 Roberts L. F., Kasen D., Lee W. H., Ramirez-Ruiz E., 2011, ApJ, 736, L21
 Sakurai A., 1960, Commun. Pure Appl. Math., 13, 353
 Sari R., Mészáros P., 2000, ApJ, 535, L33
 Sari R., Piran T., Narayan R., 1998, ApJ, 497, L17
 Sekiguchi Y., Kiuchi K., Kyutoku K., Shibata M., 2011, Phys. Rev. Lett., 107, 051102

Shibata M., Suwa Y., Kiuchi K., Ioka K., 2011, *ApJ*, 734,
L36

Tan J. C., Matzner C. D., Mckee C. F., 2001, *ApJ*, 551,
946